Investigation of deuterium trapping and release in the JET ITER-like wall divertor using TDS and TMAP

Likonen, J.

2019-05

Likonen , J , Heinola , K , De Backer , A , Baron-Wiechec , A , Catarino , N , Jepu , I , Ayres , C F , Coad , P , Koivuranta , S , Krat , S , Matthews , G F , Mayer , M & Widdowson , A 2019 , ' Investigation of deuterium trapping and release in the JET ITER-like wall divertor using TDS and TMAP ' , Nuclear Materials and Energy , vol. 19 , pp. 166-178 . https://doi.org/10.1016/j.nme.2019.02.031

http://hdl.handle.net/10138/301465
https://doi.org/10.1016/j.nme.2019.02.031

Nuclear Materials and Energy 19 (2019) 166–178

Contents lists available at ScienceDirect

Nuclear Materials and Energy

journal homepage: www.elsevier.com/locate/nme

Investigation of deuterium trapping and release in the JET ITER-like wall divertor using TDS and TMAP

J. Likonen[a,*], K. Heinola[b], A. De Backer[c], A. Baron-Wiechec[c], N. Catarino[d], I. Jepu[c,e], C.F. Ayres[c], P. Coad[c], S. Koivuranta[a], S. Krat[f,g], G.F. Matthews[c], M. Mayer[f], A. Widdowson[c], JET Contributors[h,1]

[a] VTT Technical Research Centre of Finland, P.O. Box 1000, FIN-02044 VTT, Finland
[b] University of Helsinki, P.O. Box 64, 00560 Helsinki, Finland
[c] CCFE, Culham Science Centre, Abingdon, Oxon OX14 3DB, UK
[d] IPFN Instituto Superior Técnico, Universidade de Lisboa, 1049-001 Lisboa, Portugal
[e] National Institute for Laser, Plasma and Radiation Physics (NILPRP), Magurele 077125, Romania
[f] Max-Planck-Institut für Plasmaphysik, EURATOM Association, Boltzmannstr. 2, D-85748 Garching, Germany
[g] National Research Nuclear University (MEPhI), Kashirskoe Road 31, Moscow 115409, Russia
[h] EUROfusion Consortium, JET, Culham Science Centre, Abingdon OX14 3DB, UK

ARTICLE INFO

Keywords:
Fuel retention
JET
TDS

ABSTRACT

Selected set of samples from JET ITER-Like Wall (JET-ILW) divertor tiles exposed both in 2013–2014 and 2011–2014 has been analysed using Thermal Desorption Spectrometry (TDS). The deuterium (D) amounts obtained with TDS were compared with Ion Beam Analysis (IBA) and Secondary Ion Mass Spectrometry (SIMS) data. The highest amount of D was found on the top part of inner divertor which has regions with the thickest deposited layers. This area resides deep in the scrape-off layer. Changes in plasma configurations between the first (2011–2012) and the second (2013–2014) JET-ILW campaign altered the material migration towards the inner and the outer divertor corner increasing the amount of deposition in the shadowed areas of the divertor base tiles. D retention on the outer divertor tiles is clearly smaller than on the inner divertor tiles. Experimental TDS spectra for samples from the top part of inner divertor and from the outer strike point region were modelled using TMAP program. Experimental deuterium profiles obtained with SIMS have been used and the detrapping and the activation energies have been adjusted. Analysis of the results of the TMAP simulations enabled to determine the nature of traps in different samples.

1. Introduction

Erosion of the JET main chamber wall by hydrogen isotopes and other impurities leads to migration and deposition of wall material together with hydrogen isotopes mainly at the inner divertor as observed in recent post mortem analysis of JET-ILW plasma facing components (PFCs) [1]. The resulting co-deposited layers will be the main source for the accumulation of in-vessel tritium (T) inventory in ITER. ITER as a licensed nuclear facility has an administrative safety limit for in-vessel of 1 kg to limit the risks of release of mobilisable tritium during accidents [2]. Regular periods of baking of the first wall at 240 °C and divertor at 350 °C have been planned to be implemented in ITER. The efficiency of baking is, however, affected by thick co-deposited layers formed especially at the inner divertor [3]. In addition, the impurities in the co-deposited layers, such as oxygen and carbon, or Be/W mixed layers formed on the divertor tiles may have an effect on the release of fuel from the layers by creating new trapping sites for hydrogen isotopes [4].

In JET-ILW, the main chamber consists of solid Be limiters, which are in direct contact with the plasma, i.e. exposed to ion and Charge exchange neutral (CX) fluxes as well as to Edge-localised modes (ELMs) and transient events. In addition, in the main chamber there are recessed limiters made of W-coated carbon fibre composite (CFC) tiles, and the main chamber inner wall is fully covered with Be-coated Inconel tiles. Both the recessed limiters and the inner wall are not in direct plasma contact, i.e. they are exposed only to CX flux. The divertor

* Corresponding author.
E-mail address: jari.likonen@vtt.fi (J. Likonen).
[1] See the author list of X. Litaudon et al. 2017 Nucl. Fusion 57 102001.

https://doi.org/10.1016/j.nme.2019.02.031
Received 6 October 2018; Received in revised form 21 February 2019; Accepted 21 February 2019

consists of W-coated CFC tiles and load bearing tiles made of solid W. Gas balance measurements at JET performed during the first operational phase in 2011–2012 (ILW-1) have shown a factor of 10–20 reduction in the long term fuel retention resulting from the change of wall material from the all-carbon (JET-C) to the JET-ILW material combination [1,5]. Post-mortem analyses of divertor tiles retrieved during the 2012–2013 shutdown showed a reduction by a factor of >18 in the global fuel retention rate when compared to JET-C [1]. Moreover, the post-mortem analyses showed that the overall deposition pattern at the divertor had changed completely; during JET-C the thickest deposits were at both divertor corners and during the DTE1 campaign in 1997–1998 most of the retention occurred below the divertor [6] whereas in JET-ILW deposition occurred mainly on top of the inner divertor. This indicated that the erosion and deposition processes had changed in JET-ILW. The difference between operations with JET-ILW and with JET-C is probably due mostly to lack of chemical sputtering in JET-ILW. Firstly, greatly reduced chemical sputtering in the main chamber reduces the amount of Be entering the plasma and the scrape-off layer (SOL) and being transported to the top of the inner divertor. Secondly, the lack of chemical sputtering means there is negligible re-erosion of these (reduced) deposits followed by transport to the bottom of the divertor and into the shadowed regions. Global impurity migration code WallDYN has demonstrated strong deposition on the apron of Tile 1 and little deposition elsewhere on the rest of the W divertor [7,8].

The ILW-1 campaign concentrated on plasma scenarios most relevant for ITER, i.e. the strike points were on Tiles 3 and 5. The ILW-2 campaign, however, focussed on high power and high density plasma scenarios [9] with the inner strike points (ISP) on Tiles 3 and 4, and the outer strike points (OSP) on Tile 6. In addition, the ILW-2 operations ended in a hydrogen campaign.

The present work continues the retention studies using the TDS technique by analysing JET divertor tiles removed from the vessel after the ILW-2 experimental campaign. Comparison of retention data obtained with TDS is made with data obtained by various ion beam analysis techniques (IBA) and secondary ion mass spectrometry (SIMS).

2. Experimental methods

2.1. JET-ILW campaigns

Overall plasma times for ILW-1 and ILW-2 were similar: 19/19.4 h of total plasma time of which 13/14.2 h were the divertor phase and 6/5.2 h the limiter phase. In the ILW-1 campaign the performance was gradually expanded with commissioning phases and a programme of combined scenario development with a strong focus on ITER critical plasma-wall interaction issues. The ILW-1 campaign contained a limited number of high current pulses with plasma currents up to 3.5 MA, magnetic field up to 3.2 T and Neutral Beam Injection (NBI) heating up to 26 MW combined with Ion Cyclotron Resonance Heating (ICRH) up to 3.5 MW [10]. During the last two weeks of ILW-1 operations, identical H-mode plasmas with D were executed to study the material migration and the fuel retention under typical H-mode plasma conditions. In order to accumulate a significant divertor fluence of 5.25×10^{26} Dm^{-2}, 151 identical discharges ($B_t = 2.0$ T, $I_p = 2.0$ MA, $P_{aux} = 12$ MW) were executed. The ILW-2 campaign consisted of a larger number of high power pulses with plasma currents up to 4 MA, magnetic field up to 3.7 T, and NBI heating power up to 27 MW, ICRH up to 7 MW and Lower Hybrid Current Drive (LHCD) heating power up to 3 MW [11]. ILW-2 ended in a hydrogen (H) campaign and a programme with varied plasma configurations. Approximately 300 ILW-2 pulses were performed with H plasmas, which corresponds to ~10% of the total number of JET ILW-2 pulses and 0.6 h of plasma time.

Fig. 1 shows the poloidal cross section of the ILW divertor and higlights all the plasma-facing divertor tiles and samples that were analysed in this work. The plasma strike point distributions on the divertor tiles during ILW-1 and ILW-2 campaigns are shown in Fig. 2. During ILW-1 the ISP was predominantly on the vertical surface of Tile 3. There were some discharges with the ISP at the bottom of Tile 1 and on the sloping part of Tile 4. In ILW-2 the ISP was mainly on Tile 3 and on the sloping part of Tile 4. The OSP in ILW-1 was mainly on bulk W Tile 5 but some discharges had the OSP on Tile 6. During ILW-2 the OSP was mainly on the sloping part of Tile 6.

2.2. Sample preparation

The JET-ILW W-coated CFC divertor tiles consist of ~25 μm thick W coatings with ~3 μm thick Mo interlayers for erosion/deposition studies on CFC tiles. These tiles have a layer structure of CFC (bulk)/Mo (3 μm)/W (12 μm)/Mo (4 μm)/W (4 μm). The bulk W Tile 5 will be investigated as part of future work. The tiles used in the present study are:

- Tile 0 (identification HFGC 13N RH) exposed in ILW-1 + ILW-2
- Tile 0 (HFGC 14N LH) exposed in ILW-2
- Tile 1 (14ING1C) exposed in ILW-2
- Tile 3 (2IWG3A) exposed in ILW-1 + ILW-2
- Tile 4 (2BNG4C) exposed in ILW-2
- Tile 6 (14BNG6D) exposed in ILW-1 + ILW-2
- Tile 7 (14ONG7A) exposed in ILW-1 + ILW-2
- Tile 8 (14ONG8A) exposed in ILW-1 + ILW-2.

Some of the tiles were exposed for one campaign only (Tiles HFGC 14N, 1, 3, 4 and 6) whereas the others (HFGC 13N, 7 and 8) were exposed for two campaigns.

Samples for the present studies were cut from each tile using a coring drill; the drill had an outside diameter of 20 mm and produced a core sample of 17 mm in diameter [12]. A poloidal line of holes was drilled every 20 mm across the tile. For TDS analyses two topmost discs with thicknesses of ~1 mm were cut from the cored samples from their plasma-facing sides. The resulted TDS amounts for D represent a D depth profile of 0 to 1 mm (disc with W-coating and bulk CFC) and 1.5 mm to 2.5 mm (only bulk CFC) the offset of 0.5 mm being due to the thickness of the saw blade. Samples are identified by tile number (Tile n) and then by location (m) as shown in Fig. 1, and are referred to as e.g. 1/9, i.e. sample 9 from Tile 1.

The cross-sectional samples for SEM were prepared by cutting the cored sample poloidally and placing it into cold mounting epoxy (Epofix, Struers). A W-shaped metal clip (made of Al) was put into the epoxy in order to improve the electrical contact between the sample and SEM sample holder. Typically three sample pieces were placed in the epoxy. Polishing of the studied cross-section was done using Tegrasystem polishing system (Struers) with pre-programmed preparation method.

2.3. Analysis methods

TDS system at CCFE manufactured by Hiden Analytical Ltd (TPD Workstation type 640100) was applied to cored divertor tile samples (see Fig. 1) with a thickness of typically 1 mm. The details of the TDS instrument used have been reported extensively in a recent article [13]. TDS analyses were made in an ultra-high vacuum (UHV) system with a base pressure typically of $\sim 10^{-9}$ mbar. The samples were annealed with a linear ramp rate (10 K/min) from room temperature (RT) up to 1000 °C. The temperature of the sample surface is measured with an infrared pyrometer (RAYTEK model RAYMM2MLSF1L). The released gases were measured with a line-of-sight quadrupole mass spectrometer as a function of time and annealing temperature. The TDS data was collected for mass-to-charge ratios corresponding to various molecules, e.g. H_2, HD, D_2, DT, T_2 and evaporated Be. The D signal was calibrated with an ion implanted D reference sample and the calibration procedure has been explained in detail in Ref. [13] and only a short description

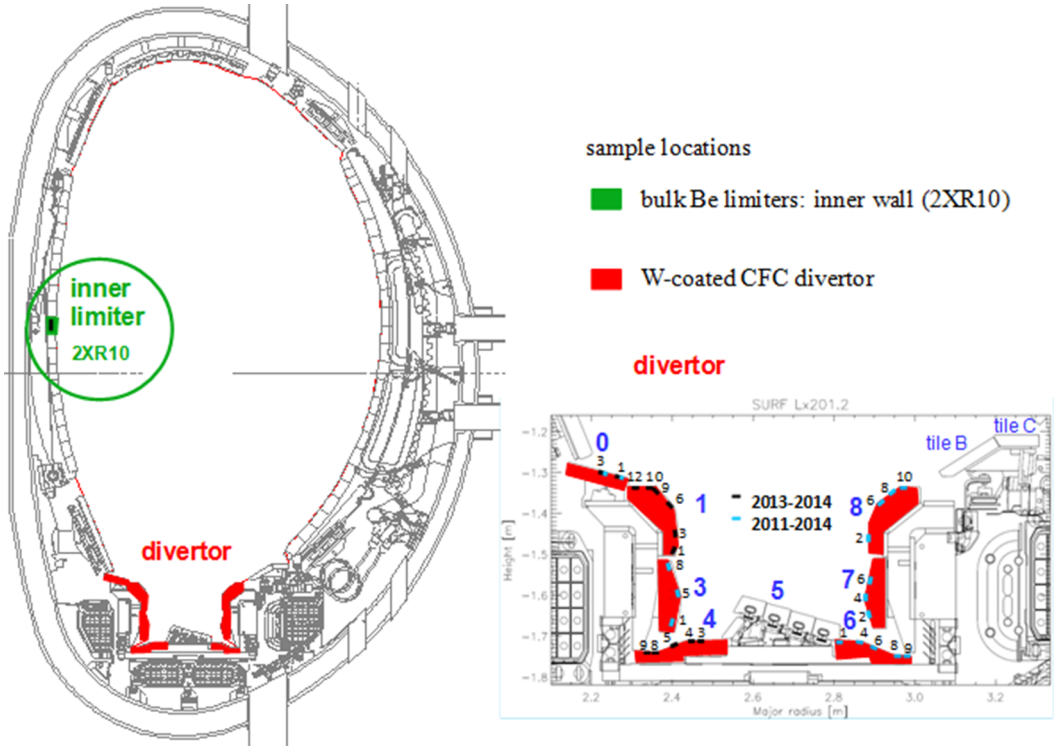

Fig. 1. Cross-section of the JET-ILW main chamber and the divertor. Location of the inner wall bulk Be limiter specimen highlighted in green. The divertor W-coated CFC tiles highlighted in red and the tile numbering from Tile 0 to Tile 8 is from the high field to the low field side, correspondingly. TDS sample locations are colour coded showing the exposure period. Samples are identified by tile number (Tile n) and then by location (m) and are referred to as e.g. 1/9, i.e. sample 9 from Tile 1. (For interpretation of the references to colour in this figure legend, the reader is referred to the web version of this article).

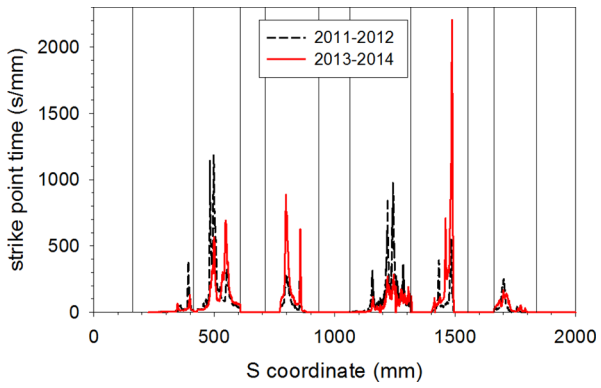

Fig. 2. Strike point distribution for ILW-1 (2011–2012) and ILW-2 (2013–2014).

will be given here. Polycrystalline W samples were implanted with a 30 keV D^+ beam to a dose of 5.8×10^{16} cm^{-2} at the University of Helsinki. The energy chosen is high enough for creating sufficient amounts of implantation-induced defects for trapping D in W at RT. Hydrogen has high diffusivity in W, so the retained D is in the implantation-induced defects (mainly vacancy-type defects), or in intrinsic defects, which can trap hydrogen at RT. During the implantation the remained D in solute sites can be considered to be diffused away from the bulk region of the sample once the implantation has finished. Detailed analysis on the 30 keV/D implantation-induced defect creation and the D retention has been provided in [14]. The absolute amount of the retained D in the implanted samples was determined experimentally with Time-of-flight Elastic Recoil Detection Analysis (TOF-ERDA) technique. The obtained result was 3.5×10^{16} D/cm^2, which is sufficient D amount for TDS. The calibration procedure used applies only for D and only rough estimations e.g. on T amounts can be made.

IBA measurements were made both at IST (Lisbon) and at IPP (Garching). At IST, 2.5 MV Van de Graaff accelerator was applied in the nuclear resonance analysis (NRA) using ^{3}He ions at an energy of 2.3 MeV for determining the amounts of deuterium [15]. At IPP, the NRA measurements were performed using 4.5 MeV ^{3}He beam [16]. In both cases D(^{3}He,p)^{4}He reaction was used detection of deuterium.

SIMS measurements were made using a double focusing magnetic sector instrument VG Ionex IX-70S at VTT. A 5 keV O_2^+ primary beam with a current of 500 nA was used [12]. D-implanted Be, Mo and W samples, which were analysed with Heavy Ion Elastic Recoil Detection Analysis (HI-ERDA) at University of Helsinki, were used for quantification of the SIMS measurements for deuterium.

The cross-sections of specimens were analysed by scanning electron microscopy (SEM) and energy dispersive X-ray (EDX) using a TESCAN Mira3 XMH FE-SEM microscope equipped with an X-Max 80 EDS detector from Oxford Instruments. The electron beam was operated at 10–30 kV.

3. Results

3.1. Inner divertor

3.1.1. Horizontal region – Tile 0 and Tile 1 apron

Tile 0 and the top horizontal part (apron) and the top plasma facing surface of Tile 1 were deep in the SOL during ILW-2 and thick impurity layers were formed by the erosion of the main wall Be limiters. Moreover, D fuel was co-deposited in these layers.

A selection of about 30 samples cut from the W-coated CFC divertor tiles removed in 2014 shutdown were analysed with TDS. These samples represent a selection of specimen, which had been exposed in JET for ILW-2, or for ILW-1 + ILW-2. Thicknesses of the co-deposited Be layer on top of W/Mo coatings is shown in Fig. 3. The thickest co-deposited layers are found on Tiles 0 and 1 but there is a deposition band

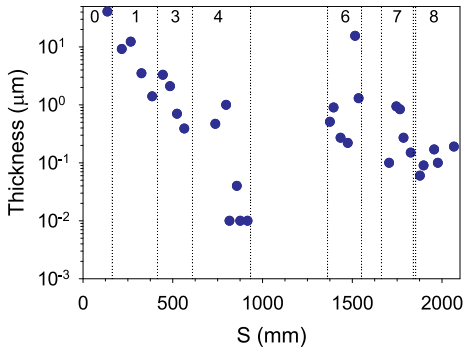

Fig. 3. Thickness of co-deposited layers on top of W/Mo coatings.

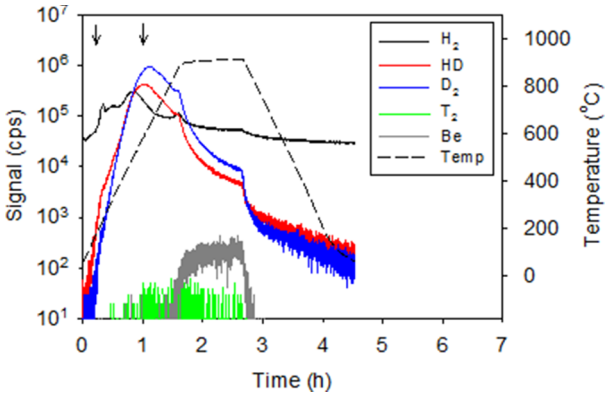

Fig. 4. TDS spectra and annealing temperature as a function of time for sample 0/1 (exposed for ILW-1 + ILW-2).

with thickness of ~15 μm on the outboard of the OSP location on Tile 6.

Fig. 4 shows TDS spectra for H_2, HD, D_2, T_2 and evaporated Be together with the sample temperature for the sample 0/1 exposed in ILW-1 + ILW-2. This specific sample has a thick Be co-deposited layer with a thickness of ~40 μm [12] (see Fig. 3) and with C and O impurities in the range of ~10^{19} at/cm^2 (see Table 1). The desorption spectra are fairly broad and desorption of HD starts at ~90 °C whereas D_2 starts to be released at slightly higher temperature (~110 °C). This could be due to the two week H campaign at the end of ILW-2 and the higher absorbed energies during ILW-2 [17]. The effect of H campaign at the end of ILW-2 can be seen in SIMS depth profiles which show clearly smaller near surface D signal and a surface peak for H signal [17]. SIMS results demonstrate that the dominant species used in the plasma operations are also found in the deposits. In the case of sample 0/1 exposed only in ILW-1 both HD and D_2 started to desorb at the same temperature (~110 °C). The HD and D_2 spectra for samples 0/1 are rather similar except that the ILW-1 sample has a peak for HD and D_2 signals at ~440 °C. The HD and D_2 signals have been deconvoluted using Origin software. The Be release from both samples 0/1 starts at higher temperatures at ~900 °C. T_2 release appeared to be very small, though. A release of Be is also observed at TDS maximum temperature. This observed Be release stays nearly at a constant level until the heating is stopped. Be signal will not give the full amount of Be in the sample as it is well below the melting temperature. It is only indicative of Be being present on the sample.

The total D amount (6.3 × 10^{18} at/cm^2) in sample 0/1 exposed in ILW-1 + ILW-2 is obtained by integrating over the HD and D_2 signals and using the calibration factor determined with the ion implanted reference sample. The D_2 signal has a broad release maximum at ~610 °C but both D_2 and HD signals have a clear bump, or shoulder in the shape of the release spectrum at ~240 °C as highlighted with vertical arrows in Fig. 4. This side peak is due to loosely bound deuterium on the surface. A similar peak in H_2 signal can also be observed at this temperature.

Deuterium is not desorbed only as a D_2 molecule but there is a significant release of HD molecules at mass 3 (~19% of the total D atoms released). The shape of the HD signal is quite similar to that of the D_2 signal but its maximum is at slightly lower temperature. H in HD molecule is both due to H in the JET samples, as indicated by SIMS measurements, H due to air exposure and due to H originating as a background in the vacuum of the TDS system. Background H in the current TDS analysis chamber has been studied extensively in Ref. [13]. However, the JET samples contain hydrogen and typically there is a H_2 peak above the background level in the H_2 signal in the TDS spectra [13]. Some test measurements were also made, and signals for masses

Table 1
Composition of the surface layers on the TDS samples measured with ion beam techniques [35]. D amount measured with TDS is also given.

Sample	D_2 (10^{15} cm^{-2})	Be (10^{15} cm^{-2})	C (10^{15} cm^{-2})	O (10^{15} cm^{-2})	D_2 (10^{15} cm^{-2}), TDS
HFGC/1 (2011–2014)	6155	257,480	13,954	24,062	6300
1/10	3079	66,040	4533	9691	3423
1/9	3917	75,187	3352	10,200	11,000
1/6	2444	16,500	1500	2800	5060
1/3	2445	13,400	1000	2400	5450
1/1	1538	6250	550	–	3700
3/8	2080	22,400	4700	–	4280
3/5	902	11,400	4000	–	1940
3/1	757	2897	1800	–	3040
4/9	1576	1760	3640	–	2400
4/8	3155	5330	8600	4000	4700
4/5	95	570	1100	–	268
4/3	297	350	600	–	1460
6/1	247	770	405	–	471
6/4	67	1925	1850	2500	1040
6/6	11	1970	1900	–	27
6/8	610	29,500	4000	–	1620
6/9	786	7075	1000	–	1270
7/2	107	1100	865	–	5310
7/4	147	1183	1170	–	6385
7/6	218	2315	750		6450
8/2	342	234	220		949
8/6	488	750	645		2120
8/8	430	675	975		1680
8/10	416	740	550		1450

14–20 were followed during the annealing. The CD signal (mass 14) contains also the doubly charged N_2 ions which are not possible to separate from CD ion with the present system. The results indicate that these signals are about two orders of magnitude smaller in intensity than the D_2 signal. Thus, it can be concluded that these signals do not contain D in significant amounts.

In Fig. 4 is also shown the release of T_2 molecules. A small T_2 signal was recorded with TDS at low temperatures where the desorption starts at ~260 °C. It appears that the T_2 release takes place at somewhat higher temperature than the D_2 release. Since there is much less T (~5×10^{14} at/cm^2) [18] as compared to H or D, it could be expected that a T atom reaching the surface might have a higher probability of combining with a H or D atom than with a T atom. The TDS spectrometer cannot presently separate HT from a D_2 molecule so it is not possible to tell if there is release of HT. On the other hand, DT signal at mass 5 was minuscular. It is still not clear why there is strong HD emission but no DT release. One reason could be that the T maximum release takes place at high temperature where D release is decreasing, and the maximum release of T is already extremely low. There is a second release component for T_2 at much higher temperature (at ~780 °C). The first component represents release of T from loosely bound traps whereas the higher temperature component could be due to release of high energy DD generated T atoms that are implanted deeper into the sample [5].

Fig. 5 shows TDS result for a sample from the horizontal part of Tile 1 (sample 1/10) exposed in ILW-2. The spectra are similarly fairly broad as was observed with sample 0/1 exposed in ILW-1 + ILW-2 (Fig. 4). Some Be and T_2 is also released during annealing. The co-deposited layer on sample 1/10 has a thickness of ~9 μm so it is clearly thinner than on sample 0/1. The C impurity amount in sample 1/10 is also much smaller than in sample 0/1 (see Table 1). Main differences between the TDS spectra for samples 0/1 and 1/10 is that D release occurs at lower temperatures for sample 1/10 and that TDS spectra for sample 0/1 have two release maxima (~560 and 710 °C) whereas the spectra for sample 1/10 have three maxima (~220, 440, 595 °C). The release occurring at lower temperatures for sample 1/10 is related to thinner co-deposit on the sample; it has been observed earlier that the thickness of the co-deposit has a significant effect on D release [3]. In addition, as mentioned above, there was a H campaign at the end of ILW-2 which resulted in H surface peak in SIMS depth profiles. The H surface peak observed in the SIMS depth profile for sample 1/10 was thinner than for sample 0/1.

The structure of the co-deposited layer on sample 1/10 was analysed with SEM. Fig. 6 shows a typical Back-Scattered Electron (BSE) image obtained of that layer. In general, heavier elements such as W appear as bright regions whereas the light elements appear darker. The SEM image shows clearly a layered structure of the co-deposit. In addition, there are cracks and some particles embedded in the co-deposited layer. The layers are thin with a thickness less than one micron.

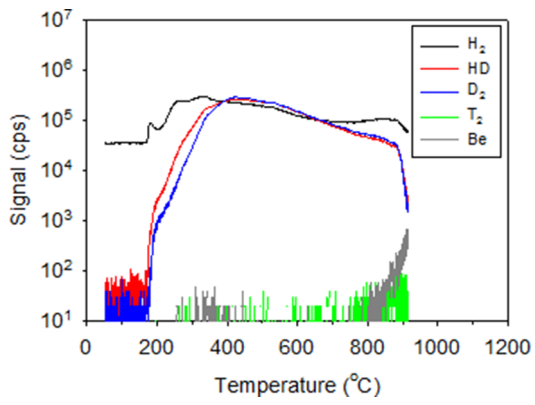

Fig. 5. TDS spectra and annealing temperature for sample 1/10.

There is clearly a contrast difference between the layers indicating that a heavy element (Ni, W) is mixed in the deposition. The layered structure is related to JET operation history and/or discrete events. Similar layered structure of the co-deposit was observed also for a sample from the same poloidal location but exposed for ILW-1 [19]. Microbeam IBA (μ-IBA) [20,21] has revealed that deposition and retention of D is microscopically inhomogeneous on plasma facing surfaces. Deposition of D was found in microscopical pits, cracks and depressed regions found on the surface. This D found on the surface imperfections can be related to loosely bound D, which is then released at low temperatures during the TDS annealing. D trapped deep in the samples with concentration profiles reaching up to the W coating has been observed both with IBA, μ-IBA and SIMS measurements. Possible diffusion mechanism for this deep trapping is along the columnar structures of the W and Mo coating. This D trapped deeper in the TDS samples is released at higher annealing temperatures.

3.1.2. Vertical region –Tile 1 and Tile 3

The TDS spectra for sample 1/9 from the upper vertical region of Tile 1 exposed for ILW-2 are fairly broad with three D release maxima whereas the spectra from the lower vertical region of Tile 1 (sample 1/3) are clearly narrower with two release maxima (see Fig. 7). Release of HD and D_2 occurs at same temperatures for both samples and also the first release maximum are at same temperatures (~400 °C). The second release maximum for D (at ~515 °C) is clearly more intense for sample 1/9 than for sample 1/3 indicating that the concentration of deep trap is higher for sample 1/9. Be release from sample 1/9 was more intense than from sample 1/10. The amount of Be released decreased from the upper vertical region of Tile 1 towards the lower vertical region which coincides with previous results obtained with IBA (see Table 1) [1]. Although Be is released, it will not be the full amount because the maximum annealing temperature is well below the melting point of Be. T_2 release also decreased when going from the upper vertical region of the tile towards the lower vertical region. The upper vertical region of Tile 1 has a co-deposited layer with a thickness of ~10 μm whereas there is some deposition at the lower vertical region of Tile 1 but there is no continuous layer. The D amount is clearly higher for sample 1/9 (~1×10^{19} cm^{-2}) than for sample 1/3 (~5.5×10^{18} cm^{-2}, see Table 1). The C amount is ~3 times higher in sample 1/9 than in sample 1/3 (see Table 1). TDS spectra for sample 1/6 located at the upper vertical region of Tile 1 have also the second release maxima (at ~550 °C) indicating that the concentration of the deep trap is high. Sample 1/6 has clearly thinner co-deposited layer than sample 1/9 Be amount being ~5 times smaller. The D and C amounts are also smaller in sample 1/6 than in sample 1/9. The second release maxima for HD and D_2 signals for sample 1/6 are clearly stronger than for sample 1/3.

Tile 3 was exposed both for the ILW-1 and ILW-2 campaign in 2011–2014. During the ILW-1 the ISP was predominantly on Tile 3 whereas during the ILW-2 it was mainly on Tile 4 (see Fig. 2). Optical microscopy indicates that on the top part of the Tile 3 there has been minor erosion of the W coating and in some areas also the Mo layer has partly been eroded [22]. On the other hand, at the top of Tile 3 deposits with a thickness of ~3 μm are observed on the surface overlaying the eroded W/Mo layers. The thickness of the Be co-deposit decreases to ~1 μm at the lower part of the tile [12]. TDS spectra for HD and D_2 molecules from the bottom (sample 3/1) and from the top (sample 3/8) of Tile 3 are shown in Fig. 8. The spectra for sample 3/8 are clearly broader than for sample 3/1 but both HD and D_2 have the maximum release at ~570 °C. Sample 3/8 contains also more D than sample 3/1. Release of Be was also observed with the TDS especially from the sample near the top region of the tile whereas near the bottom hardly any Be was released (see Table 1). When the TDS spectra for samples from Tile 3 (exposed for ILW-1 + ILW-2) are compared with those from Tile 1 (exposed for ILW-2) one difference is that D is released at higher temperatures from Tile 3 than from Tile 1 (400 vs. 570 °C, respectively). D retention is somewhat higher on Tile 1 than on Tile 3 but C amounts

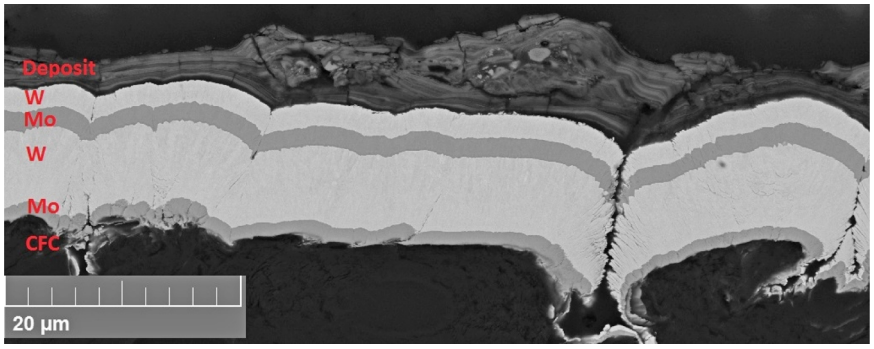

Fig. 6. SEM image for sample 1/10.

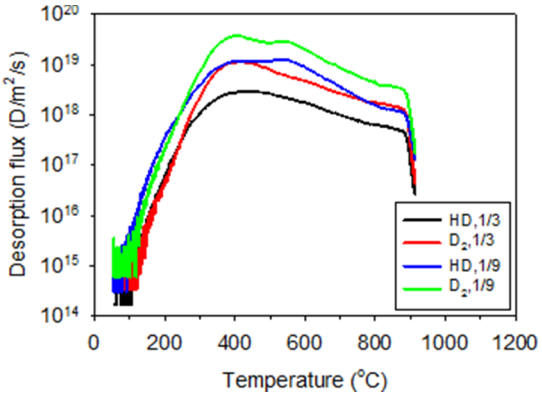

Fig. 7. TDS spectra for sample 1/3 and 1/9.

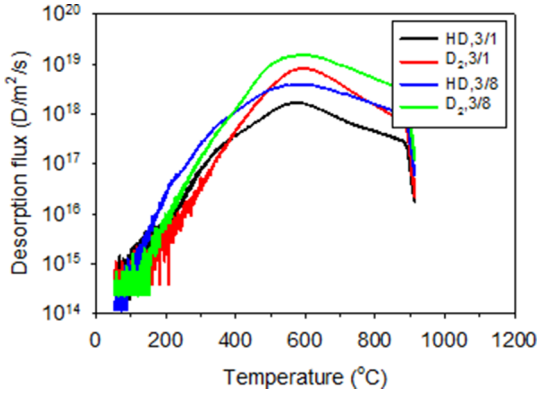

Fig. 8. TDS spectra for sample 3/1 from the bottom of Tile 3 and for sample 3/8 from the top of Tile 3.

are comparable on both tiles. Both tiles have a co-deposit on the top part of the tile with similar thicknesses so the thickness of the co-deposit cannot be the reason for different release temperatures. One possible explanation is that ISP was on Tile 3 and main locations for ISP on Tile 3 were at S = 498 mm and S = 548 mm during ILW-2. Sample 3/1 (S = 585 mm) was mainly then in the private flux region (PRF) during these discharges and sample 3/8 (S = 445 mm) mainly in the SOL. Sample 3/6 (S = 485 mm) from near the centre of Tile 3 also showed D release at high temperature similarly to the other samples from Tile 3. The absorbed energy on Tile 3 is somewhat higher than on Tile 1 indicating higher tile temperatures [17]. So, during the discharges with the ISP on Tile 3 D in traps with low energy may have been released whereas the traps with higher energies were not emptied.

The D amounts determined with TDS are compared in Fig. 9 with those obtained with NRA and SIMS for tiles removed after ILW-2. Fig. 9 shows the D amount as a function of the S-coordinate for Tiles 0, 1 and

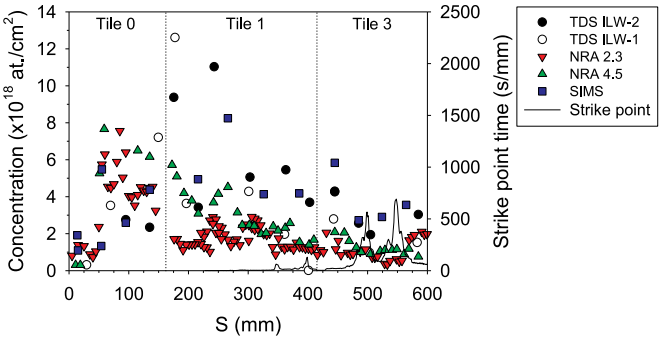

Fig. 9. D amount on Tiles 0, 1 and 3 measured with TDS, NRA and SIMS. TDS ILW-1 corresponds to TDS analyses made from ILW-1 tiles. NRA and SIMS results are for ILW-2. The OSP distribution is also shown.

3. The highest D amounts are on Tile 0 and on the apron of Tile 1. TDS and SIMS show higher results on Tiles 1 and 3 than NRA whereas on Tile 0 NRA results are typically higher than SIMS and TDS data. Fig. 9 also gives the TDS results for ILW-1 tiles. The results are somewhat scattered for Tiles 0 and 1. In the case of Tile 3 the ILW-2 results are higher than the ILW-1 results but this is due to that Tile 3 was exposed for both campaigns. In Ref. [17] are given the impurity (Be, C, O) amounts measured with NRA also for the ILW-1 campaign. The deposition pattern changed during ILW-2 from that for ILW-1 due to changes in the plasma geometry. During ILW-1 impurities were deposited mainly on the apron and the upper vertical part of Tile 1 whereas during ILW-2 deposition extended further down on the plasma facing surface of Tile 1.

3.2. Divertor base

During ILW-2 more low delta discharges, i.e. strike points on Tiles 4 and 6, were applied. The ISP on Tile 4 was mainly on the sloping part which changed the migration pattern allowing more transport towards Tile 4. There is some deposition on Tile 4 and the measured Be amount is up to 10 times higher at the deposition region (S = 760 mm) after ILW-2 when compared to ILW-1. Be and D deposition extend also to the plasma shadowed region at the inner corner of the divertor [22]. Fig. 10 shows TDS spectra for sample 4/3 which is on the top horizontal part and for sample 4/5 which is located at the top of the sloping part of Tile 4. The spectra are fairly broad with D release maxima at temperatures ~320, ~500 and 600 °C which correspond quite well with the release temperatures for Tile 1. In addition, sample 4/3 has a small peak at ~800 °C. The spectra for sample 4/5 are quite different from those for sample 4/3. Overall D amount is smaller in sample 4/5 and the D release maximum at the lower temperature (~320 °C) is smaller than the D release maximum at the higher temperature (~570 °C). This means that the low energy trap has been emptied during the plasma operations which is possibly due to that the ISP has been on the same location as

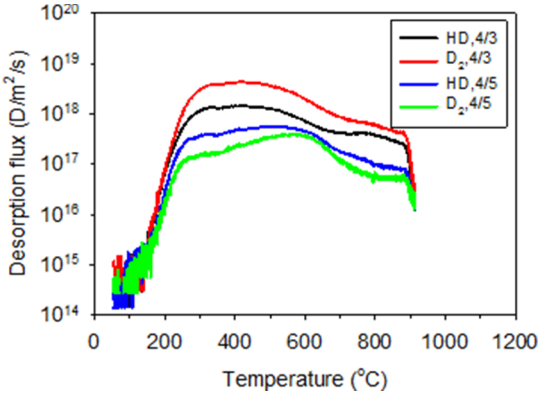

Fig. 10. TDS spectra and annealing temperature for sample 4/3 and 4/5.

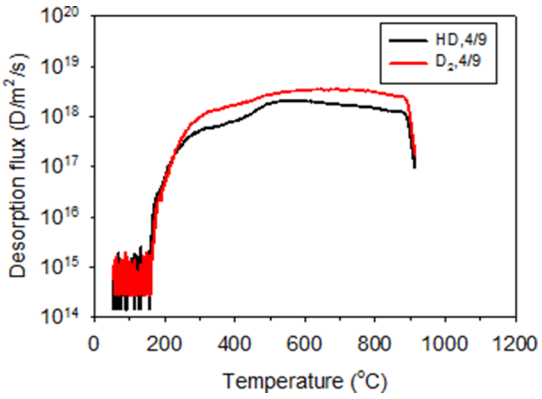

Fig. 11. TDS spectra and annealing temperature for sample 4/9.

sample 4/5. The ISP was mainly at S = 800 and 860 mm. H amount on sample 4/5 is higher than on sample 4/3 even though D amount is smaller. The higher H signal for sample 4/5 is real and not due to e.g. poor vacuum because at the end of the annealing cycles background H levels are the same for both samples. The HD signal is also higher than D_2 signal in sample 4/5 indicating higher H content in the sample than compared with sample 4/3. The TDS spectra for sample 4/9 located in the shadowed region of the tile look different from those for samples 4/3 and 4/5 (see Fig. 11). The spectra are broad with three release maxima at ~380, 610 and 750 °C. Corresponding TDS spectra for sample 4/8 exposed in ILW-1 (not shown here) are also very broad, but the D amount is ~7 times smaller than for sample exposed in ILW-2. The ISP time was ~3 times higher at S = 800 mm for ILW-2 than for ILW-1. The transport mechanism towards the shadowed region of Tile 4 during these discharges when the ISP at S = 800 mm is similar for both campaigns and as a consequence line of sight transport from the ISP location to relatively cooler remote surfaces. Impurity fluxes are different as observed in the IBA analyses [22]. However, the broad TDS spectra for the samples located at the remote corner of Tile 4 are thus typical for this region where the amounts of D co-deposited are dependent on the impurity transport. Be and T_2 release were negligible for all the analysed samples from Tile 4 exposed for ILW-2.

During ILW-2 the OSP was mainly on the sloping part of Tile 6 at S = 1487 mm whereas during ILW-1 it was mainly on the bulk W Tile 5. Similarly to Tile 4, a deposition band outboard of the OSP location with a thickness ~6 times greater than for ILW-1 was observed at S = 1511 mm [15]. SIMS shows that the thickness of the deposit was ~15 μm (see Fig. 3) [12]. However, for most of the samples from Tile 6 the thickness of the deposit is less than 1 μm.

Figs. 12 and 13 show the TDS spectra for samples 6/4 (from top of the sloping part), 6/6 (from the sloping part) and 6/8 (from the shadowed region). The TDS spectra for sample 6/4 have release maxima at

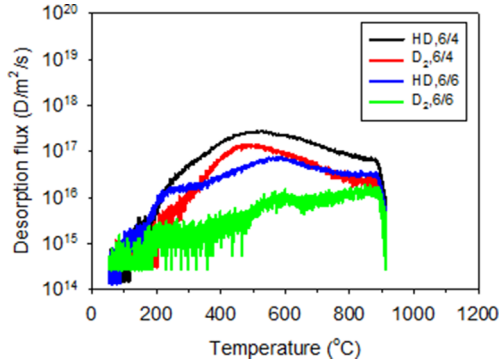

Fig. 12. TDS spectra and annealing temperature for sample 6/4 and 6/6.

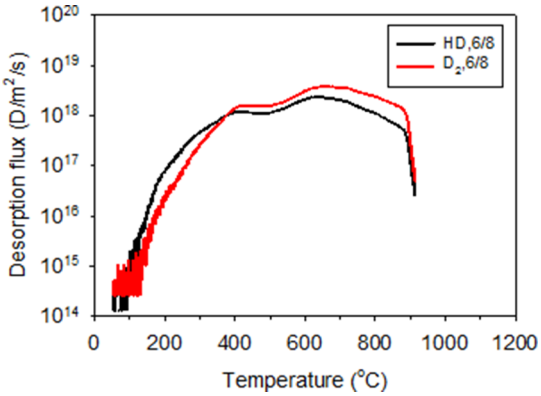

Fig. 13. TDS spectra and annealing temperature for sample 6/8.

~470 °C (D_2) and ~490 °C (HD). The HD and D_2 signals from sample 6/6 which was located near the OSP have three release maxima at ~345, ~540 and ~800 °C. Note that the D amount near the OSP is smaller than elsewhere on Tile 6. Be and T_2 release from samples 6/4 and 6/6 was small similarly to samples 4/3 and 4/5 (Fig. 10). T_2 release was clearly smaller for samples 4/3 and 6/4 than for samples 4/5 and 6/6, correspondingly. When comparing the spectra for sample 4/3 and 6/4 (top sloping parts of inner/outer divertor corner tile) with each other it can be observed that the low temperature release maximum for D at ~330 °C is more intense for sample 4/3 than for sample 6/4. The temperatures for the release maxima for sample 6/4 are higher than for sample 4/3. This could be due to somewhat higher Be and C amounts in sample 6/4 but also due to temperature differences between Tiles 4 and 6. The TDS spectra for sample 6/8 from the shadowed region (Fig. 13) are broader than the spectra for samples 6/4 and 6/6. Similar broad spectra were also observed on shadowed region of Tile 4 (Fig. 11). The release maxima for Tile 6 samples were found at temperatures ~420, ~610 and ~740 °C which are rather comparable to those for sample 4/9. The main difference between the inner divertor corner (Tile 4) and the outer corner (Tile 6) is that there is a thick deposit (>10 μm) on Tile 6 shadowed region. In this region, also Be and T_2 release during TDS annealing was observed.

An example of the type of deposit found on the sloping surface of Tile 6 is shown in Fig. 14. Fig. 14(a) shows an area with a thin deposit (thickness <1 μm). The deposited layer is not, however, continuous as shown in Fig. 14(b). There are layers only in the plasma shadowed regions. The insert in Fig. 14(b) shows a layered structure (thickness <1 μm). In addition, the thin layers contain bright particles which are most likely W.

Poloidal distribution of D on base Tiles 4 and 6 together with the strike point distributions is shown in Fig. 15. Comparison is made between TDS, NRA and SIMS data. In the case of Tile 4 there is more D near the shadowed corner and the D amount decreases as a function of

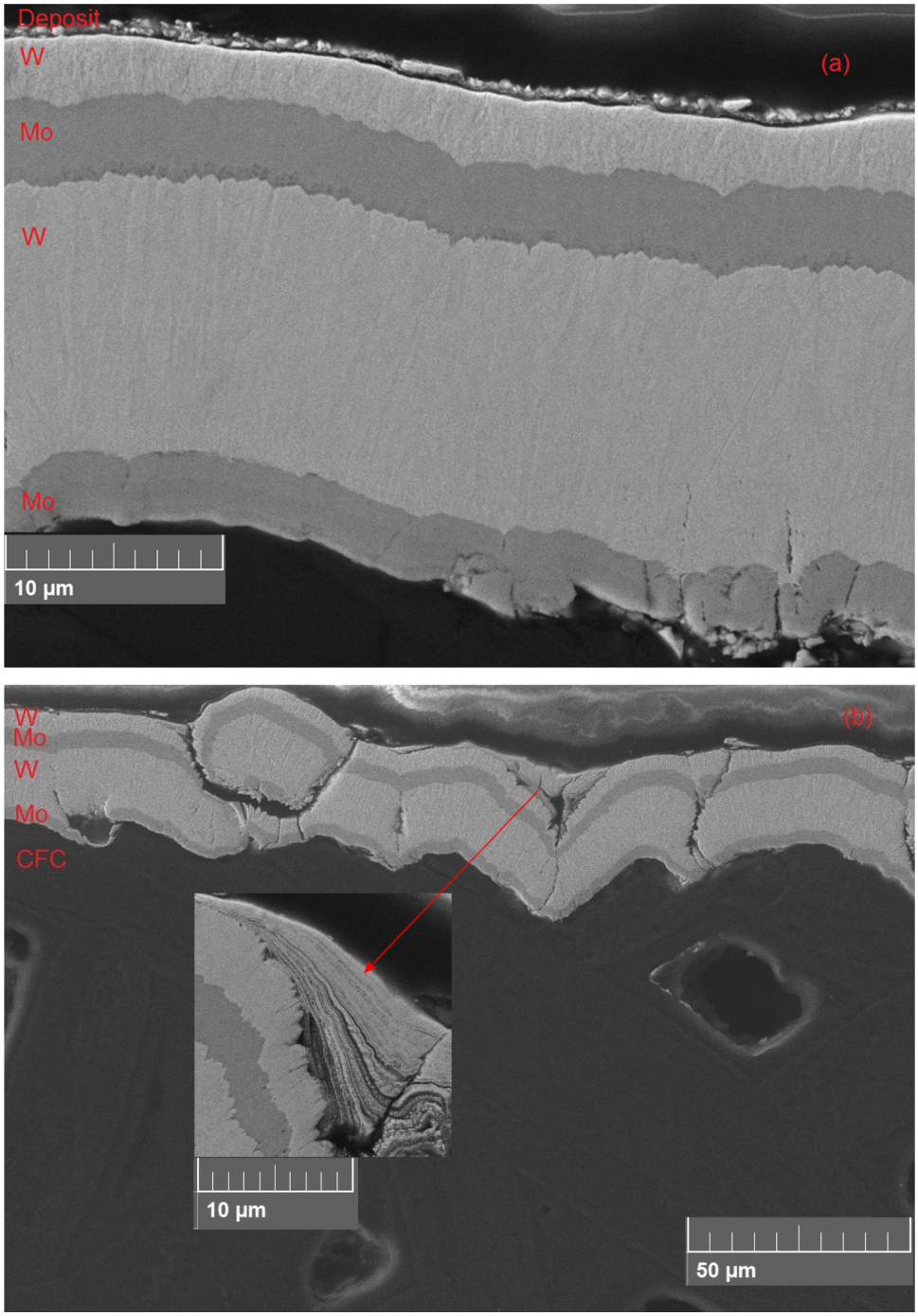

Fig. 14. SEM images from sample 6–5. (a) BSE image from an area with a deposited layer, (b) BSE image from a plasma shadowed area with a layered deposit.

the *S*-coordinate. There is also clear difference between ILW-1 and ILW-2 as there was much less D after ILW-1. The difference is due to different plasma geometries as explained in chapter 2.1. There is some scatter between the different analysis techniques but overall agreement is good [12,15,16]. The D distribution shows a minimum near the ISP at $S \sim 810$ mm as indicated by NRA 4.5MeV, SIMS and TDS results. However, at the ISP location $S = 857$ mm TDS and SIMS show higher D amounts than for neighbouring samples. It can be that D was deposited after those discharges with the ISP at $S = 857$ mm. It is not, however, known when the ISP was at $S = 857$ mm so it would require further analysis of the ISP position with JET pulse number.

Tile 6 was exposed for ILW-1 + ILW-2 and there was no significant OSP induced heating affecting D retention during ILW-1 because the OSP time on Tile 6 during ILW-1 was much lower than during ILW-2. The D amount after ILW-2 is relatively low on the top horizontal part of Tile 6, except the two SIMS data points. Near the main OSP location there is a minimum in the D amount for all the measurement techniques indicating D release near the OSP due to higher absorbed energies during ILW-2 [17]. NRA shows a maximum at the OSP location $S = 1460$ mm, though. The D amount increases towards the shadowed region of Tile 6. The D retention at the divertor inner and outer corner regions are not symmetric as there is more D retention poloidally at the inner than at the outer divertor corner.

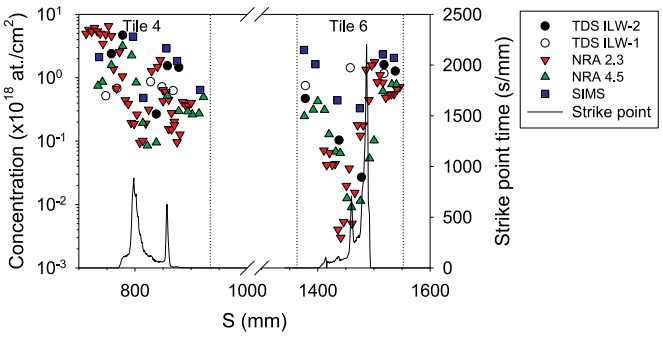

Fig. 15. D amount on Tiles 4 and 6 measured with TDS, NRA and SIMS. TDS ILW-1 corresponds to TDS analyses made from ILW-1 tiles. NRA and SIMS results are for ILW-2. The OSP distribution is also shown.

3.3. Outer divertor

Outer divertor Tiles 7 and 8 were exposed for both ILW-1 and ILW-2 campaigns and only small erosion is visible on Tiles 7 and 8. During ILW-1 there was no significant OSP induced heating affecting the D retention and only minor deposits were observed on these tiles. The exposure of Tiles 7 and 8 for two campaigns, different OSP location during ILW-2 and the higher absorbed energies in ILW-2 had a significant effect on the D retention.

TDS spectra for sample 7/2 located near the bottom of the tile are very sharp the maximum release occurring at ~560 °C (see Fig. 16). The corresponding spectra for sample 7/4 located near the centre of Tile 7 are clearly broader with a release maximum at ~500 °C. The Be and T_2 were also released in the case of sample 7/2 but for sample 7/4 Be and T_2 release were smaller. The TDS spectra for sample 7/6 are also relatively broad. The main release peak is at somewhat lower temperature (~480 °C) than for sample 7/4 but there is a smaller release component at temperature ~630 °C. The highest release temperature for sample 7/2 is due to the OSP induced heating of Tile 7 which emptied the lower energy traps of D during JET operation. The temperature for the maximum D release decreases as the distance from the OSP increases. C and Be amounts on Tile 7 are somewhat lower than on Tile 6.

TDS spectra for samples from the plasma-facing surface of Tile 8 are also fairly broad (see Fig. 17). Maximum D release occurs at ~450 °C for both samples and there is a second release maximum at ~640–700 °C. The spectra from near the top of Tile 8 are also similar to those in Fig. 17. Be release is the highest for sample 8/2 even though the Be amount increases towards the top of the tile [17]. The TDS spectra for sample 8/10 (see Fig. 18) located on the apron are completely different from those from the lower vertical regions of the tile. The D release spectra are narrow and the main release maximum is very sharp at temperature ~640 °C indicating that the low energy traps have

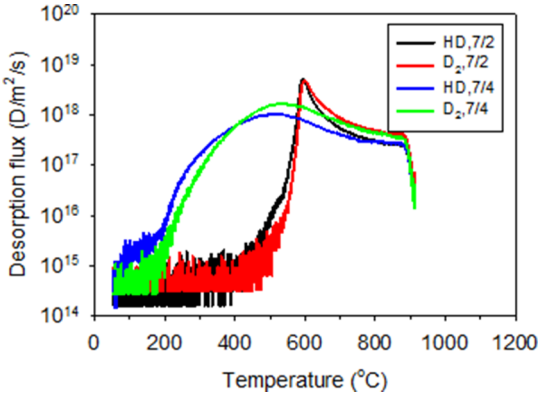

Fig. 16. TDS spectra and annealing temperature for sample 7/2 and 7/4.

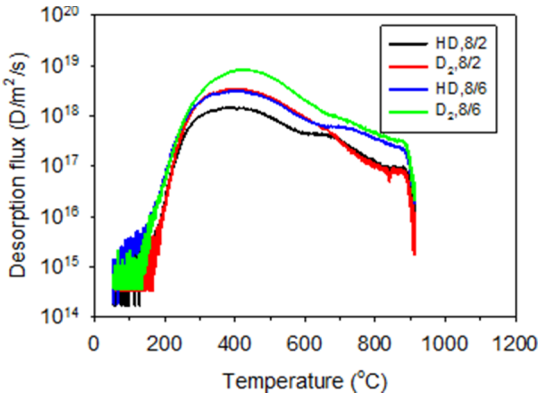

Fig. 17. TDS spectra and annealing temperature for sample 8/2 and 8/6.

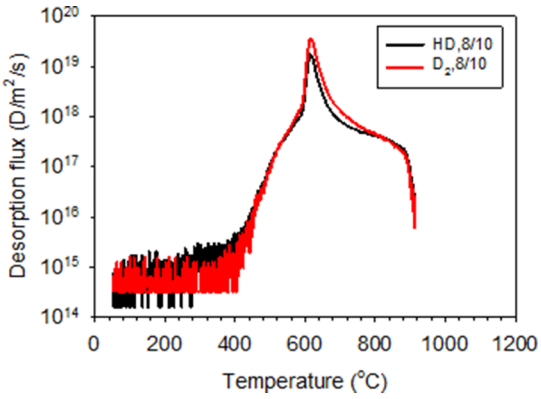

Fig. 18. TDS spectra and annealing temperature for sample 8/10.

been emptied during the plasma operations. There are also smaller release maxima at ~530 and ~790 °C. The impurity (Be, C) amounts are comparable on the plasma facing surface and the top horizontal surface (see Table 1) so this cannot explain the differences between the TDS spectra from the vertical regions and the apron. Moreover, apron of Tile 8 is deep in the SOL. However, W erosion of the apron of Tile 8 was observed during ILW-1 and ILW-2 which could be due to both ELMs and interaction of ICRF with the top of Tile 8 [23]. W erosion of the apron of Tile 8 released most likely loosely bound D and emptied low energy traps.

Fig. 19 shows the poloidal D amount as a function of the S-coordinate for Tiles 7 and 8. 4.5 MeV NRA, TDS and SIMS indicate lower D amount near the bottom of Tile 7 due to the OSP location. 2.3 MeV NRA shows, however, somewhat different distribution than the other techniques. TDS and SIMS results near the centre of the Tile 7 are somewhat higher than the NRA data which could be due to greater

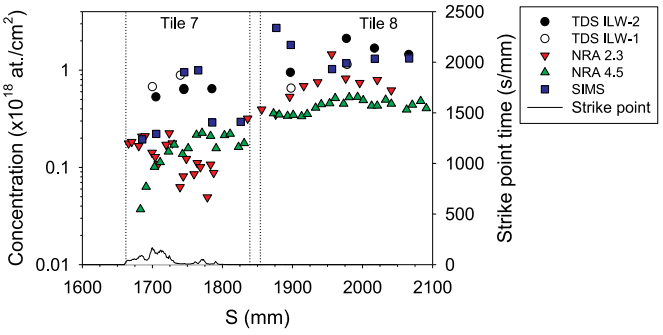

Fig. 19. D amount on Tiles 7 and 8 measured with TDS, NRA and SIMS. TDS ILW-1 corresponds to TDS analyses made from ILW-1 tiles. NRA and SIMS results are for ILW-2. The OSP distribution is also shown.

analysis depth of these techniques. It has been observed that D trapping at the W-Mo and Mo-W interfaces is significant and dominates D retention in Tile 7 [21]. The depth at which this D retention occurs thus beyond the detection depth of NRA. The TDS results for D in ILW-1 are somewhat higher for Tile 7 than the ILW-2 results which is most likely due to higher absorbed powers during ILW-2 resulting in increased D desorption during JET operation. The D amount on Tile 8, which was deep in the SOL during the plasma operations, is somewhat higher than on Tile 7. The Tile 8 TDS and SIMS results for D are again somewhat higher than corresponding NRA results which is most likely due to D retention deep in the surface as in the case of Tile 7. TDS results for ILW-1 are somewhat lower than for ILW-2 indicating a gradual build-up of D retention as for both campaigns Tile 8 was in the deep SOL. The 4.5 MeV NRA results are slightly lower than the 2.3 MeV results even though higher beam energy should probe greater depths so the difference may be due to different analysis procedures and different analysis positions toroidally.

4. Modelling

As discussed in the previous section, the D retention strongly depends on the formation of a co-deposited layer, its composition and the plasma exposure history. The position of the D release maximum in TDS spectrum is usually associated with the hydrogen energy required for detrapping from a trap but the peak position depends also on the layer thickness, the D depth distribution and the annealing rate. These can be due to impurities and defects in the materials microstructure. The desorption peak is also affected on the depth which the D depth profile extends to and on the nature of the corresponding trapping and detrapping and retrapping dynamics.

There are three methods to determine if different D release peaks observed in the TDS spectra can be associated with particular trap types with specific binding energies and to identify these traps by comparison between the binding energy revealed by TDS and the theoretical calculations: (1) run several TDS measurements varying the temperature ramp rate, (2) use a model for the D desorption rate which takes into account the diffusion of deuterium and the recombination rate at the surface for the temperature ramp defined by the TDS experiment, and (3) combination of (1) and (2). In our case, the first and third method are excluded since the tokamak samples used in the present study represent a unique set of samples with very limited availability.

A first attempt of the modelling of desorption rates during TDS performed on JET-ILW samples was done by using TMAP7 [24]. TMAP [25] is a 1-D model which can include several atomic species and several H isotopes. It models the diffusion of the species including the trapping and release from static point traps characterised by their concentrations, size and corresponding hydrogen binding energy. TMAP can also take into account mechanisms such as radioactive decay, dissociation and recombination rates at the surface, heat source and heat diffusion.

In this work, we used a simple model based on the properties of Be [26]. The model includes deuterium diffusion to the surface and trapping/detrapping in point traps. We used same values for deuterium diffusion and solubility as in Ref. [26]. The D concentration in the traps results from trapping and detrapping. The rate for detrapping depends on the temperature as $\exp(-E_a/kT)$ where E_a is the activation energy for detrapping and is the sum of the binding energy and the migration energy for diffusion.

The desorption is diffusion limited and the concentration at the surface is fixed by the Sievert's law. It must be pointed out that, in preliminary simulations we observed that a more complex surface model, i.e. a concentration dependent recombination rate used in [26], mainly changes the peak shape. When compared to the simple surface model, the complex surface model first slows down the desorption as the deuterium concentration at the surface must increase in order that the desorption can start and it prolongs the desorption at large temperatures because the desorption is slowed down when the deuterium surface concentration becomes small at the end of the desorption peak. In our study, the shape of the peaks suggests much more complex trapping properties than in [26], probably due to the inhomogeneity of the codeposited layers, the presence of impurities and the non-uniformity of the codeposit thickness (as revealed by the SIMS and SEM studies).

The relevant TMAP equations are summarised below. Eq. (1) is for the mobile D atoms and (2) for the trapped D concentration in traps of type "k",

$$\frac{\partial C}{\partial t} = -D\frac{\partial^2 C}{\partial x^2} - \sum_k \frac{\partial C_{t_k}}{\partial t} \tag{1}$$

$$\frac{\partial C_{t_k}}{\partial t} = \frac{\alpha_t C^e_{t_k}}{N} C - \alpha_{r_k} C_{t_k} \tag{2}$$

where $C^e_{t_k} = C^0_{t_k} - C_{t_k}$, $\alpha_t = D/\lambda^2$ and $\alpha_{r_k} = \upsilon_0 e^{-E_{t_k}/kT}$. The parameters are:

C is the concentration of mobile deuterium atoms, C_{t_k} is the concentration of D atoms in the traps of type "k", $C^e_{t_k}$ is the concentration of empty traps of type "k", $C^0_{t_k}$ is the total concentration of traps of type "k", D is the diffusivity of deuterium, E_{t_k} is the trapping energy of the traps of type "k", α_t is the trapping rate coefficient of deuterium atoms, α_{r_k} is the release rate coefficient for trapped D atoms in trap "k", ν_0 is the Debye frequency (10^{13} s^{-1}), N is the lattice atom density (atom/m^3), λ is the lattice parameter (m), k is the Boltzmann's constant and T is temperature (K).

The initial deuterium concentration is the trap concentration times the trap filling. For this work, the traps are considered to be 100% filled and the depth profile is based on our SIMS results. The concentration of traps of type "k" is based on the SIMS profile rescaled to correspond to the amount of deuterium associated with one TDS peak as given in Table 2. One exception is sample 2XR10C3-50 where the profile can be decomposed in two exponentials which have been associated to two types of traps. Eventually, only the binding energy of the traps is adjusted such that the calculated peak location is the same that the TDS ones.

In this study, four samples have been considered 2XR10C3/50 (see Fig. 1), 1/10 (exposed for ILW-2), 6/5 (exposed for ILW-1) and 6/6

Table 2
Comparison and summary of results for the four samples included in the modelling study.

	2XR10C3/50	1/10	6/5	6/6
Location in JET vessel	Inner limiter	Inner divertor	Shadowed surface of the divertor base	
Plasma exposure period	ILW-1	ILW-2	ILW-1	ILW-1 +ILW-2
Isotope from plasma	D only	H and D	D only	2x D and H
composition	Be	Co-deposit on W layer (and Mo), D–Be with C and O		
SEM		Fig. 6	Fig. 14	
SIMS:	0.2	8	1	1
D depth profile (μm)	surface peak and power law	surface peak + step + low background		Surface peak + power law
TDS retention ($1e^{18}D/cm^2$)	0.1	3.4	1.4	0.027
TDS peaks (°C)	530	220, 440, 595	240, 405	345, 540, 800

Table 3
Parameters for the TMAP simulations of four samples. The solubility and diffusivity for D are based on the Be properties [24]. The trap concentrations are based on the measured SIMS depth profiles (except for 2BNG6C-5 where a simple exponential profile is assumed). For sample 2XR10C3/50 the traps can be separated spatially as suggested by the surface peak (Gaussian concentration) and the power law of the SIMS profile (Fig. 20a). C_i^0 is pre-exponential factor. In the case of samples 1/10, 6/5 and 6/6 traps cannot be separated spatially. The total concentration profiles are given in Fig. 20a and X_i^0 is the fraction of this profile associated with trap of type *i*. The deuterium diffusion coefficient is $8.0 \times 10^{-9} \times e^{(-0.364/kT)}$ m^2/s and the deuterium solubility is $2.3 \times 10^{22} \times e^{(-0.174/kT)}$ /(m^3 $Pa^{1/2}$) where *T* is the temperature in Kelvin.

Sample		Trap 1	Trap 2	Trap 3
2XR10C3-50	Ci0	0.9	0.02	
	Characteristic depth distance (μm)	0.035	0.250	
	E_a (eV)	1.634	1.714	
	Temperature peak (°C)	530	620	
1/10 (ILW-2)	TDS T_{peak} (°C)	220	440	595
	X_i^0	40	40	20
	E_a (eV)	0.95	1.15	1.45
	Temperature peak (°C)	300	515	680
6/5 (ILW-1)	TDS T_{peak} (°C)	240	440	560
	C_i^0	0.03	0.08	0.005
	E_a (eV)	0.9	1.2	1.4
	Temperature peak (°C)	260	460	565
6/6 (ILW-1 + ILW-2)	TDS T_{peak} (°C)	345	540	800
	X_i^0	5	53	42
	E_a (eV)	1.2	1.6	2.3
	Temperature peak (°C)	290	645	>1000

(exposed for ILW-1 + ILW-2). A comparison of these four samples is summarised in Table 2. The first one (2XR10C3/50) comes from near the centre (poloidally) of the Be inner wall guard limiter (IWGL). This region is an erosion dominated zone without deposits, so it can be considered that its properties represent bulk Be. The second one is sample 1/10 from the apron of Tile 1 and characterised by a thick co-deposit (see SEM Fig. 6), the D depth profile extends to a depth of 8 μm with a clear concentration peak at the surface. TDS shows main desorption peak at ~440 °C for sample 1/10. The third sample is sample 6/5 for which we assume a 1 μm thick co-deposit (see SEM Fig. 14) and one main desorption peak at ~350 °C with a shoulder at low temperature [18]. This sample was not exposed during the ILW-2 campaign. The last sample is sample 6/6 exposed for ILW-1 + ILW-2 campaigns has a D depth profile extending slightly less than 1 μm into the sample surface. The TDS spectrum is particularly broadened with three peaks and the maximum at ~540 °C (see Fig. 12). Outgassing of D is still detected at 1000 °C.

The parameters of TMAP simulations are given in Table 3. The deuterium depth profiles are based on SIMS results (except 2BNG6C/5) and introduced as a concentration of up to three types of filled traps in the TMAP simulations. In the case of sample 2XR10C3/50 two types of traps are spatially separated as the SIMS depth profile suggested one type close to the surface and another one deeper in the sample. The binding energies were adjusted to fit the TDS peaks. Note that samples 1/10 and 6/6 have been exposed to hydrogen plasmas at the end of ILW-2 campaign which causes a large concentration of hydrogen close to the surface and a reduced concentration of deuterium in the first 250 nm (see Fig. 20a). Hydrogen was not included in the TMAP model of this work.

TDS spectrum of the bulk Be sample 2XR10C3/50 (see Fig. 20b) is well reproduced by one main trap with a detrapping energy of 1.64 eV. This corresponds to H trapping in Be mono-vacancy according to the DFT calculations by Ganchenkova et al. [27]. According to this model stronger traps (1.7 eV) in small concentration could cause a small peak at high temperature. This trap may be related to some impurities or larger defects.

Sample 1/10 has a thick Be co-deposit and the deuterium depth profile extends to a depth of ~10 μm (see Fig. 20a). Comparison with the sample from the IWGL limiter (2XR10C3/50) shows that the TDS peak is significantly larger for sample 1/10 and that the TMAP model shows that it is not only due to the thick D profile. Indeed, the trap activation energy necessary to reproduce such a large peak in the TDS spectrum varies from 0.95 to 1.45 eV. In general, large traps are characterised by a distribution of traps [28]. In TMAP, only three types of traps are possible. The range of the activation energy suggests that even though the composition of the co-deposited layer is mainly Be, its retention properties are significantly different from the bulk Be material of the limiter. Even though the peak in the TDS spectra maxima are quite close to each other (530 and 440 °C, see Fig. 20b), we cannot attribute the D retention to mono-vacancies in the divertor sample 1/10.

A comparison of samples 6/5 and 6/6 shows that the depth profiles (see Fig. 20a) are rather similar (except reduction of D near the surface for sample 6/6) but very different TDS peak positions (see Fig. 20d) causing a shift of the activation energy from 0.9, 1.2, 1.4 to 1.2, 1.6, 2.3 eV for samples 6/5 and 6/6, respectively. In Fig. 20e are plotted the peak temperatures of deuterium outgassing as a function of the detrapping energies of the traps in the model. One can observe that as in the first order kinetic model [29], there is roughly a linear relation between the peak position and the detrapping energy but the coefficient depends on the trap concentration and more generally on the concentration profile. Note that the effective diffusion coefficient is influenced by the detrapping-retrapping process and the concentration of traps. One can observe for example that samples 6/6 and 6/5 have a low temperature release peak at similar positions but the detrapping energy is 35% larger for sample 6/6 than for 6/5. This is due to the two orders of magnitude larger trap concentration close the surface in sample 6/5 compared to sample 6/6 which reduces the effective diffusion coefficient. The activation energy of second trap in sample 6/6 is consistent with a mono-vacancy and third trap can be related to vacancy clusters. Sample 6/6 is very different from sample 6/5 and one must notice that sample 6/6 was exposed for ILW-1 + ILW-2.

5. Discussion

The main material migration mechanism at JET during the ILW-2 campaign is still Be erosion at the main wall by charge exchange neutrals and transport during the X-point phase of the plasma towards the inner divertor. As in ILW-1, the HFGC tile and the top horizontal part of Tile 1 are still the main deposition areas in ILW-2. Plasma configurations for the ILW-1 and ILW-2 campaigns were different. The ISP was mainly on Tile 3 for the ILW-1 campaign whereas during the ILW-2 campaign the ISP was on Tile 4 which widened the SOL interaction with Tile 1 when compared to the ILW-1 campaign. In addition, higher input powers used during the ILW-2 campaign increased Be erosion at the main wall resulting in more material transport towards the divertor. This increased deposition on the top plasma-facing surface of Tile 1 and near the strike points on Tiles 4 and 6. The higher absorbed energies near the strike points during the ILW-2 campaign induced higher temperatures on the tiles which resulted in D out-diffusion. This can be observed especially for Tile 6. The ILW-2 campaign ended in a H campaign. This resulted in near-surface H accumulation and reduction in D amount as observed with SIMS depth profiling [12,17]. A sharp release peak at ~200 °C was observed in most of the TDS spectra (see e.g. Fig. 4). This peak was not observed in the TDS spectra for samples exposed during the ILW-1 campaign so the peaks in the TDS spectra for samples exposed during the ILW-2 could be due the H campaign during the last two weeks of the ILW-2. When TDS spectra for the ILW-1 and ILW-2 campaign are compared with each other it can be observed that in general the TDS spectra for the ILW-1 samples have release maxima at lower temperatures than the corresponding spectra for the ILW-2 samples (see [18]). This is partly related to lower absorbed energies used during the ILW-1 campaign, as higher tile temperatures in plasma wetted areas lead to D out-diffusion especially from the low energy traps. In addition, the ILW-1 spectra are somewhat narrower than the ILW-2 spectra, except for the outer divertor Tiles 7 and 8. The

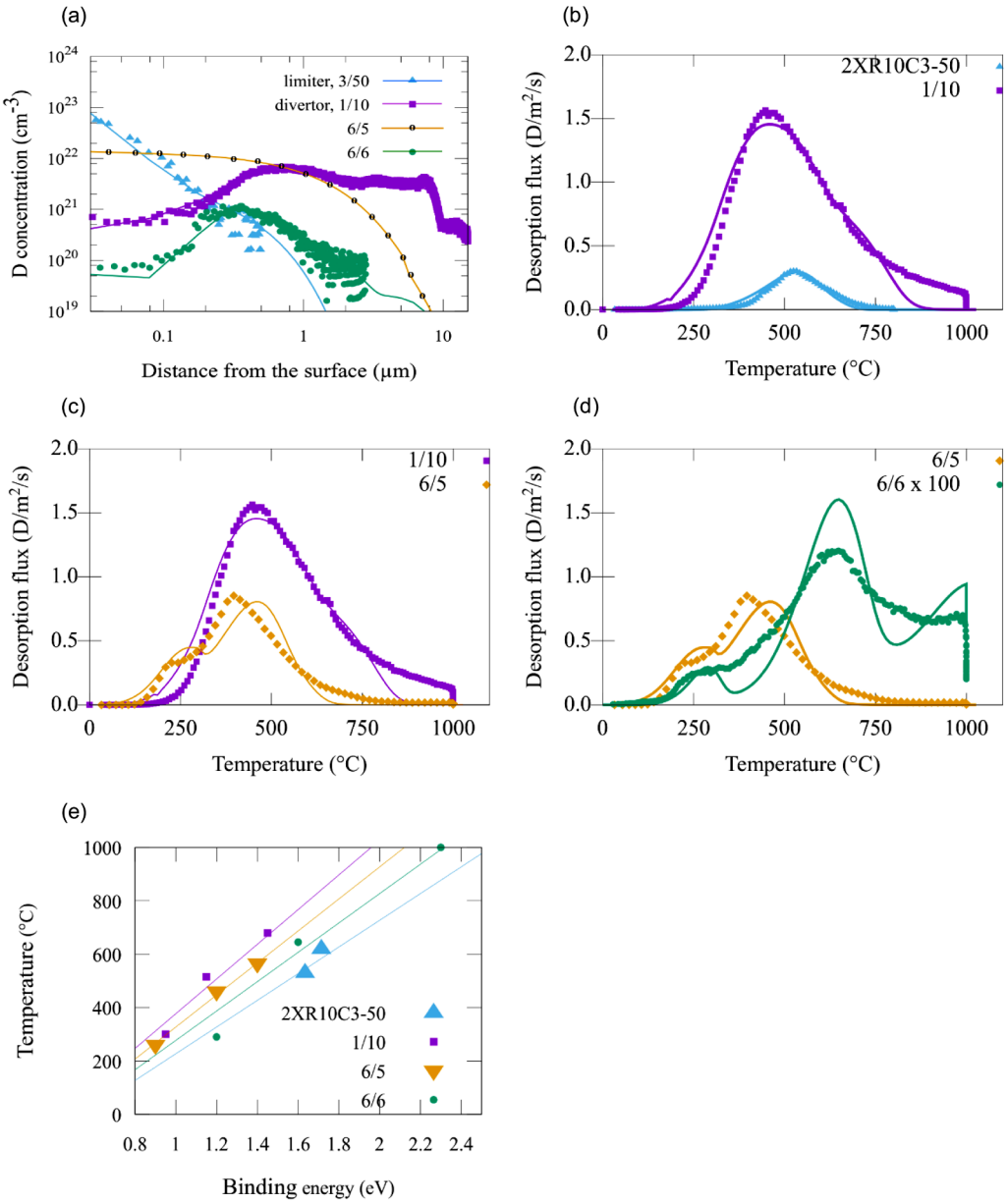

Fig. 20. (a) SIMS depth profiles for D used in TMAP simulations. For sample 6–5 an exponential profile was used because no SIMS data was available. Rescaling in case of sample 2XR10C3-50 is necessary because the sample analysed by SIMS is not the same as analysed by TDS. (b) Comparison of experimental and simulated TDS spectra between a limiter (2XR10-50) and a divertor (1/10) sample, (c) between Tile 1 (1/10) and Tile 6 (6/5) and (d) between samples 6/5 and 6/6, (e) Peak temperature of the TDS as a function of the binding energy in the TMAP model for the different samples. In Figures (b) and (c) the desorption flux needs to be multiplied by a factor of 10^{19}, and in Figure (d) by a factor of 10^{18}.

impurities (Be, C) may also have an effect on the TDS spectra. Higher Be erosion during the ILW-2 campaign increased transport towards the divertor, but also C amount in general is higher on the ILW-2 samples except on samples from Tile 1.

Further investigations are necessary to fully determine the nature of the traps but these simulations already indicate that mono-vacancies or vacancy clusters could be present. The Be-rich co-deposited layers have significantly different properties which can be due to the different impurities or the multilayer microstructure. The first two traps for sample from the apron of Tile 1 correspond well with those observed on PISCES co-deposits [23]. The high energy traps observed in JET samples could be due to impurities. From the modelling point of view, a possible or more sophisticated approach could take into account different depth profiles of traps or several material layers. There are also models in the literature which include the diffusion and annihilation of the traps (which is particularly important when the traps are vacancies [30]), saturable traps with the binding energies depending on the filling of the traps [31], extended traps characterised by a distribution of binding energies [28,32], pores open to the surface [33] and isotopic exchanges [34]. However, more sophisticated models would require a larger number of sample analysis than available for this study and more experimental characterisations of the codeposited layers and deuterium retention.

6. Conclusions

TDS has been used to analyse samples from W-coated CFC divertor tiles exposed during the ILW-2 campaign in 2013–2014. As was during the ILW-1 campaign, in ILW-2 the highest amount of deuterium was found on the regions with the thickest co-deposited layers, i.e. on HFGC tile and on the top horizontal part and at the top of plasma-facing surface of Tile 1. There is comparable D retention in the shadowed corner of Tile 4 and there is a Be-rich deposition band inboard of the ISP. The D amount decreases towards Tile 5. Tile 6 has similar Be-rich deposition band outboard of the OSP. The outer shadowed region of Tile 6 has less D retention than the shadowed region of Tile 4, though. There is clearly less deposition on the outer divertor Tiles 7 and 8 than on the inner divertor tiles. The D retention increases as a function of the S-coordinate from the bottom of Tile 7 towards the top of Tile 8. The TDS results indicate increase in the D retention outside the OSP for the outer divertor tiles when comparing results between the ILW-1 and

ILW-2 campaigns. TDS spectra for the ILW-1 and ILW-2 campaign were compared with each other and it was observed that in general the TDS spectra for the ILW-1 samples have release maxima at lower temperatures than the corresponding spectra for the ILW-2 samples. This is partly related to lower absorbed energies used during the ILW-1 campaign, as higher tile temperatures in plasma wetted areas lead to D outdiffusion especially from the low energy traps. In addition, the ILW-2 campaign ended in a H campaign which resulted in near-surface H accumulation and reduction in D amount and effected the features of the TDS spectra. The higher release temperatures for D in the ILW-2 samples due to higher absorbed energies may have an effect on the efficiency of the planned 623 K divertor bake at ITER.

Experimental TDS spectra for samples from the top horizontal part of Tile 1 and sloping part of Tile 6 were modelled with the TMAP program using a three trap model. In addition, a bulk Be sample from the IWGL limiter was used to setup the TMAP parameters. Reasonable agreement between experimental and TMAP calculations was obtained. The first two traps for sample from the apron of Tile 1 correspond well with those observed on PISCES co-deposits. The high energy traps observed in JET samples could be due to impurities.

Conflict of interest

There are no conflict of interests.

Acknowledgements

This project has received funding from Tekes – Finnish Funding Agency for Technology and Innovation (under grant 4433/31/2015) – and the European Union's Horizon 2020 research and innovation programme. This work has been carried out within the framework of the EUROfusion Consortium and has received funding from the Euratom research and training programme 2014–2018 under grant agreement no. 633053. The views and opinions expressed herein do not necessarily reflect those of the European Commission.

Supplementary materials

Supplementary material associated with this article can be found, in the online version, at doi:10.1016/j.nme.2019.02.031.

References

[1] K. Heinola, A. Widdowson, J. Likonen, E. Alves, A. Baron-Wiechec, N. Barradas, S. Brezinsek, N. Catarino, J.P. Coad, S. Koivuranta, S. Krat, G.F. Matthews, M. Mayer, P. Petersson, Long-term fuel retention in JET ITER-like wall, Phys. Scr. T167 (2016) 014075.
[2] C.A. Taylor, P. Cortes, Progress in the Safety and Licensing of ITER, Fusion Sci. Technol 64 (2013) 111.
[3] K. Heinola, J. Likonen, T. Ahlgren, S. Brezinsek, G. De Temmerman, I. Jepu, G.F. Matthews, R.A. Pitts, A. Widdowson, Long-term fuel retention and release in JET ITER-Like Wall at ITER-relevant baking temperatures, Nucl. Fusion 57 (2017) 0860024.
[4] K. Sugiyama, J. Roth, A. Anghel, C. Porosnicu, M. Baldwin, R. Doerner, K. Krieger, C.P. Lungu, Study of deuterium retention in/release from ITER-relevant Be-containing mixed material layers implanted at elevated temperatures, J. Nucl. Mater. 438 (2013) S1113.
[5] S. Brezinsek, T. Loarer, V. Philipps, et al., Fuel retention studies with the ITER-Like Wall in JET, Nucl. Fusion 53 (2013) 083023.
[6] J.P. Coad, N. Bekris, J.D. Elder, et al., Erosion/deposition issues at JET, J. Nucl. Mater. 290-293 (2001) 224.
[7] K. Schmid, K. Krieger, S.W. Lisgo, G. Meisl, S. Brezinsek, Quantitative modeling of fuel retention in the JET-C and JET-ILW wall configurations by WallDYN and predictions for ITER, J. Nucl. Mater. 463 (2015) 66.
[8] K. Schmid, K. Krieger, S.W. Lisgo, G. Meisl, S. Brezinsek, WALLDYN simulations of global impurity migration in JET and extrapolations to ITER, Nucl. Fusion 55 (2015) 053015.
[9] I. Nunes, S. Brezinsek, J. Buchanan, et al., First Results from Recent JET Experiments in Hydrogen and Hydrogen-Deuterium Plasmas, Proceedings of the 26th IAEA Fusion Energy Conference, Paper PDP-2, Kyoto, Japan, 2016, pp. 17–22 October.
[10] E. Joffrin, M. Baruzzo, M. Beurskens, C. Bourdelle, et al., First scenario development with the JET new ITER-like wall, Nucl. Fusion 54 (2014) 013011.
[11] F. Romanelli, Overview of the JET results, Nucl. Fusion 55 (2015) 104001.
[12] A. Lahtinen, J. Likonen, S. Koivuranta, A. Hakola, K. Heinola, C.F. Ayres, J.P. Coad, A. Widdowson, J. Räisänen, Deuterium retention in the divertor tiles of JET ITER-Like wall, Nucl. Mater. Energy 12 (2017) 655.
[13] A. Baron-Wiechec, K. Heinola, J. Likonen, E. Alves, N. Catarino, J.P. Coad, V. Corregidor, I. Jepu, G.F. Matthews, A. Widdowson, Thermal desorption spectrometry of beryllium plasma facing tiles exposed in the JET tokamak, Fusion Eng. Des. 133 (2018) 135.
[14] T. Ahlgren, K. Heinola, K. Vortler, J. Keinonen, Simulation of irradiation induced deuterium trapping in tungsten, J. Nucl. Mater. 427 (2012) 152.
[15] N. Catarino, N.P. Barradas, V. Corregidor, A. Widdowson, A. Baron-Wiechec, J.P. Coad, K. Heinola, M. Rubel, E. Alves, Assessment of erosion, deposition and fuel retention in the JET-ILW divertor from ion beam analysis data, Nucl. Mater. Energy 12 (2017) 559.
[16] M. Mayer, S. Krat, W. Van Renterghem, A. Baron-Wiechec, S. Brezinsek, I. Bykov, P. Coad, Y. Gasparyan, K. Heinola, J. Likonen, A. Pisarev, C. Ruset, G. de Saint-Aubin, A. Widdowson, Erosion and deposition in the JET divertor during the first ILW campaign, Phys. Scr. T167 (2016) 014051.
[17] K. Heinola, A. Widdowson, J. Likonen, T. Ahlgren, E. Alves, C.F. Ayres, A. Baron-Wiechec, N. Barradas, S. Brezinsek, N. Catarino, P. Coad, C. Guillemaut, I. Jepu, S. Krat, A. Lahtinen, G.F. Matthews, M. Mayer, Experience on divertor fuel retention after two ITER-Like Wall campaigns, Phys. Scr. T170 (2017) 014063.
[18] J. Likonen, K. Heinola, A. De Backer, S. Koivuranta, A. Hakola, C.F. Ayres, A. Baron-Wiechec, P. Coad, G.F. Matthews, M. Mayer, A. Widdowson, Deuterium trapping and release in JET ITER-like wall divertor tiles, Phys. Scr. T167 (2016) 014074.
[19] A. Baron-Wiechec, A. Widdowson, E. Alves, C.F. Ayres, N.P. Barradas, S. Brezinsek, J.P. Coad, N. Catarino, K. Heinola, J. Likonen, G.F. Matthews, M. Mayer, P. Petersson, M. Rubel, W. van Renterghem, I. Uytdenhouwen, Global erosion and deposition patterns in JET with the ITER-like wall, J. Nucl. Mater. 463 (2015) 157.
[20] H. Bergsåker, I. Bykov, P. Petersson, G. Possnert, J. Likonen, S. Koivuranta, J.P. Coad, W. Van Renterghem, I. Uytdenhouwen, A.M. Widdowson, Microscopically nonuniform deposition and deuterium retention in the divertor in JET with ITER-like wall, J. Nucl. Mater. 463 (2015) 956.
[21] H. Bergsåker, I. Bykov, Y. Zhou, P. Petersson, G. Possnert, J. Likonen, J. Pettersson, S. Koivuranta, A. Widdowson, Deep deuterium retention and Be/W mixing at tungsten coated surfaces in the JET divertor, Phys. Scr. T167 (2016) 014061.
[22] A. Widdowson, E. Alves, A. Baron-Wiechec, N.P. Barradas, N. Catarino, J.P. Coad, V. Corregidor, A. Garcia-Carrasco, K. Heinola, S. Koivuranta, S. Krat, A. Lahtinen, J. Likonen, M. Mayer, P. Petersson, M. Rubel, S. Van Boxel, Overview of the JET ITER-like wall divertor, Nucl. Mater. Energy 12 (2017) 499.
[23] Vl. Bobkov, G. Arnoux, S. Brezinsek, J.W. Coenen, L. Colas, M. Clever, A. Czarnecka, F. Braun, R. Dux, A. Huber, P. Jacquet, C. Klepper, E. Lerche, C. Maggi, F. Marcotte, M. Maslov, G.F. Matthews, M.L. Mayoral, K. McCormick, A. Meigs, D. Milanesio, I. Monakhov, R. Neu, J.-M. Noterdaeme, Th. Pütterich, F. Rimini, G. Van Rooj, G. Sergienko, D. Van Eester, ICRF specific plasma wall interactions in JET with the ITER-like wall, J. Nucl. Mater. 438 (2013) S160.
[24] G. De Temmerman, M.J. Baldwin, D. Anthoine, K. Heinola, A. Jan, I. Jepu, J. Likonen, C.P. Lungu, C. Porosnicu, R.A. Pitts, Efficiency of thermal outgassing for tritium retention measurement and removal in ITER, Nucl. Mater. Energy 12 (2017) 267.
[25] G. Longhurst, TMAP7 User Manual, INEEL/EXT-04–02352, Idaho National Engineering and Environment Laboratory, Idaho Falls, Idaho, 2008 Rev. 2.
[26] M.J. Baldwin, T. Schwarz-Selinger, R.P. Doerner, Experimental study and modelling of deuterium thermal release from Be-D co-deposited layers, Nucl. Fusion 54 (2014) 073005.
[27] M.G. Ganchenkova, V.A. Borodin, R.M. Nieminen, Hydrogen in beryllium: Solubility, transport, and trapping, Phys. Rev. B79 (2009) 134101.
[28] B.J. Merrill, M. Shimada, P.W. Humrickhouse, Simulating Tritium Retention in Tungsten with a Multiple Trap Model in the TMAP Code, J. Plasma Fusion Res. Ser. 10 (2013) 71.
[29] A.V. Fedorov, Evolution of Point Defect Clusters During Ion Irradiation and Thermal Annealing, Ph.D. Thesis University of Delft, Delft, Netherlands, 2000.
[30] R. Piechoczek, M. Reinelt, M. Oberkofler, A. Allouche, Ch. Linsmeier, Deuterium trapping and release in Be(0 0 0 1), Be(11-20) and polycrystalline beryllium, J. Nucl. Mater. 438 (2013) S1072.
[31] K. Schmid, U. von Toussaint, T. Schwarz-Selinger, Transport of hydrogen in metals with occupancy dependent trap energies, J. Appl. Phys. 116 (2014) 134901.
[32] A. De Backer, D.R. Mason, C. Domain, D. Nguyen-Manh, M.-C. Marinica, L. Ventelon, C.S. Becquart, S.L. Dudarev, Multiscale modelling of the interaction of hydrogen with interstitial defects and dislocations in BCC tungsten, Nucl. Fusion 58 (2018) 016006.
[33] S. Möller, A. Kreter, Ch. Linsmeier, U. Samm, Thermally activated reaction-diffusion-controlled chemical bulk reactions of gases and solids, Nucl. Mater. Energy 1 (2015) 1.
[34] U. von Toussaint, T. Schwarz-Selinger, K. Schmid, First-passage kinetic Monte Carlo on lattices: Hydrogen transport in lattices with traps, J. Nucl. Mater. 463 (2015) 1075.
[35] M. Mayer, S. Krat, A. Baron-Wiechec, Y. Gasparyan, K. Heinola, S. Koivuranta, J. Likonen, C. Ruset, G. de Saint-Aubin, A. Widdowson, Erosion and deposition in the JET divertor during the first ILW campaign, Phys. Scr. T170 (2017) 014051.